MiR-92a-3p Promotes Renal Injury and Fibrosis Through Facilitating M1 Macrophage Polarization via Targeting LIN28A

Mingzhi XU[1]*, Xin ZENG[1]*, Mingjiao PAN[1], Ruman CHEN[1], Yafei BAI[1], Jiqing HE[1], Chunli WANG[1], Yonghui QI[1], Qingyi SUN[1], Cuijuan WANG[1], Na AN[1]

** These authors contributed equally to this work.*

[1]Blood Purification Center, Hainan General Hospital, Hainan Affiliated Hospital of Hainan Medical University, Haikou, Hainan Province, China

Received December 18, 2023
Accepted May 7, 2024

Summary

Infiltrated and activated M1 macrophages play a role in kidney injury and fibrosis during chronic kidney disease (CKD) progression. However, the specific ways that M1 macrophage polarization contributes to renal fibrosis are not fully understood. The study seeks to investigate how miR-92a-3p regulates M1 macrophage polarization and its connection to renal fibrosis in the development of CKD. Our results revealed that miR-92a-3p overexpression increased M1-macrophage activation, iNOS, IL-6, and TNF-α expression in RAW264.7 upon LPS stimulation. LIN28A overexpression reversed these effects. Moreover, miR-92a-3p overexpression in RAW264.7 exacerbated NRK-52E cell apoptosis induced by LPS, but LIN28A overexpression counteracted this effect. MiR-92a-3p knockout in unilateral ureteral obstruction (UUO) C57BL/6 mice led to reduced renal infiltration and fibrosis, accompanied by decreased iNOS, α-SMA, IL-6, TNF-α, and increased LIN28A. In summary, our findings suggest that miR-92a-3p may play a role in promoting renal injury and fibrosis both *in vitro* and *in vivo*. This effect is potentially achieved by facilitating M1 macrophage polarization through the targeting of LIN28A.

Key words

Chronic kidney disease • Renal fibrosis • M1 macrophage polarization • miR-92a-3p • LIN28A

Corresponding author

N. An, Blood Purification Center, Hainan General Hospital, Hainan Affiliated Hospital of Hainan Medical University, No. 19 Xiuhua Road, Xiuying District, Haikou 570311, Hainan Province, China. E-mail: annacn08@163.com

Introduction

Chronic kidney disease (CKD) frequently goes undiagnosed in its early stages due to the lack of evident symptoms, affecting over 10 % of the adult population in the United States and showing a continuous increase in prevalence, especially in the presence of comorbidities [1,2]. The disease progression is notably characterized by kidney inflammation and fibrosis, conditions heavily influenced by the activity of macrophages [3]. Macrophages, which are pivotal in producing pro-inflammatory cytokines and fibrosis factors, are categorized into M1 and M2 types based on their functions [4-6]. M1 macrophages, known for their role in exacerbating inflammation, are activated by external stimuli such as LPS or IFNγ, leading to an increase in inflammatory mediators like iNOS, IL-6, and IL-12 [6,7]. In contrast, M2 macrophages, which help resolve inflammation, are stimulated by IL-4 and IL-13 to express anti-inflammatory factors such as Arg1 and IL-10 [7].

The regulatory role of microRNAs (miRNAs) in macrophage polarization is the focus of this investigation. MiRNAs are short non-coding RNA molecules that modulate various biological processes, including cell apoptosis, proliferation, and inflammation, by targeting specific mRNAs [8,9]. For example, miR-374b-5p promotes M1 macrophage activation by targeting the suppressor of cytokine signal 1 (SOCS1) during renal ischemia/reperfusion injury [10]. Hao *et al.* [11] demonstrated that LNA-anti-miR-150 reduces pro-inflammatory M1/M2 macrophage polarization,

alleviating renal interstitial fibrosis. This study particularly examines miR-92a-3p, part of the miR-17-92 cluster, is located on chromosome 13q31.3 within the third intron of the C13orf25/MIR17HG gene [12]. Notably, inhibiting miR-92a-3p can alleviate oxidative stress and pyroptosis in tubular epithelial cells (TECs) during renal ischemia-reperfusion injury (IRI) by targeting nuclear factor-erythroid 2-related factor 1 (Nrf1) [13]. Targeting endothelial miR-92a-3p has been proposed as a potential therapeutic approach to treat atherosclerosis associated with CKD [14]. Despite existing studies, the exact mechanism by which miR-92a-3p influences M1 macrophage polarization and its subsequent impact on renal fibrosis in CKD remains unclear.

This study focuses on the LIN28 protein, comprising two homologs, LIN28A and LIN28B, each sharing similar structural and functional characteristics [15]. LIN28 is known for its selective suppression of miRNA expression and its influence on cell proliferation, differentiation, and metabolic processes across various cell types [16-18]. The overexpression of LIN28A has been previously associated with enhanced tissue repair and increased glycolytic activity in human embryonic kidney cells [19]. In the context of obstructive nephropathy, adenovirus-mediated LIN28A over-expression has been effective in reducing renal fibrosis, suggesting its potential as a therapeutic target for CKD [20]. Furthermore, the LIN28B-let-7-HMGA2 axis has been identified as a regulator of M1 macrophages, indicating its possible application in immunotherapy for breast cancer [21]. Building on prior research which identified LIN28A as a target of miR-92a-3p, this study aims to further elucidate the role of the miR-92a-3p/LIN28A axis in the regulation of M1 macrophage polarization and its impact on renal fibrosis during the progression of CKD.

The study aimed to investigate the effects of the miR-92a-3p/LIN28A axis on M1 macrophage activation in LPS-stimulated RAW267.4 cells, apoptosis in LPS-induced NRK-52E cells, and kidney pathology in mice with unilateral ureteral obstruction (UUO). The goal is to identify new treatments for renal interstitial inflammation.

Materials and Methods

Cell culture and chemical treatment

The mouse macrophage cell line RAW264.7 and rat kidney tubular epithelial cell line NRK-52E were acquired from the cell bank of the Chinese Academy of Sciences in Shanghai, China. These cell lines were cultured in DMEM (cat. no. D6046; Sigma-Aldrich, St. Louis, MO, USA) supplemented with 10 % FBS and 1 % penicillin-streptomycin (Gibco, USA) in a 5 % CO_2 atmosphere at 37 °C. To induce M1 macrophage activation in RAW264.7 cells, a stimulation with 100 ng/ml LPS (L2880; Sigma-Aldrich) was performed for 24 h.

Cell transfection

The miR-92a-3p mimic and mimic negative control (mimic NC), as well as the miR-92a-3p inhibitor and inhibitor NC, were synthesized by GenePharma Corporation in Shanghai, China. To achieve LIN28A gene overexpression, the LIN28A gene was cloned into pcDNA3.1 plasmids, resulting in the generation of plasmids for LIN28A overexpression (pcDNA3.1-LIN28A). Empty pcDNA3.1 plasmids were used as a NC for this overexpression. Transfection of RAW264.7 cells was performed using 50 μM of miR-92a-3p mimics or inhibitor and 1 μg of LIN28A overexpression plasmids, following the manufacturer's protocols for Lipofectamine® 2000 from Invitrogen in Carlsbad, CA, USA.

Luciferase reporter assay

To assess the direct binding ability between miR-92a-3p and the LIN28A mRNA 3′-UTR, a dual-luciferase reporter assay was conducted. Initially, GenePharma Corporation constructed recombinant pmirGLO plasmids that contained both the wild-type (WT) and mutant (MUT) versions of the LIN28A 3′-UTR. Subsequently, 293T cells were co-transfected with miR-92a-3p mimics or mimics NC along with either the WT or MUT-type LIN28A plasmids, using Lipofectamine 2000 reagent for efficient transfection. The luciferase activity of each experimental group was measured using the Dual-Luciferase Reporter Assay System (Promega, Madison, WI). To ensure accuracy, the value of firefly luciferase activity was normalized to Renilla luciferase activity, which served as an internal control for transfection efficiency.

Co-culture of NRK-52E cells and RAW264.7

The experiment involved co-culturing RAW264.7 cells or RAW264.7 cells transfected with miR-92a-3p mimics or miR-92a-3p mimics + pcDNA3.1-LIN28A with LPS-induced NRK-52E cells using a Transwell chamber with a 0.4 μm pore size. In detail, 1 ml of NRK-52E cells (1×10^4 cells) induced by 2 μg/ml LPS or without LPS induction were seeded in the bottom plate of the Transwell

chamber. After 4 h, 1 ml of untransfected or transfected RAW264.7 cells (1×10^4 cells) were added to the upper chamber. Consequently, the co-cultured cells were divided into five groups, which were as follows: NRK-52E, NRK-52E + LPS, NRK-52E + LPS + RAW264.7, NRK-52E + LPS + (RAW264.7 + miR-92a-3p mimics), and NRK-52E + LPS + (RAW264.7 + miR-92a-3p mimics + pcDNA3.1-LIN28A) groups. Following a 24-h co-incubation period, NRK-52E cells were harvested for further analysis.

Flow cytometry

NRK-52E cells from various experimental groups were seeded into six-well plates and treated with trypsin. After washing with PBS, the cells were collected by centrifugation and resuspended in 100 µl of binding buffer (BD Pharmingen, San Diego, CA, USA). Subsequently, the cells were stained with 5 µl of Annexin V-FITC and 5 µl of propidium iodide (BD Pharmingen) for 15 min at room temperature in the dark. The percentage of apoptotic cells was analyzed using flow cytometry (BD, FACSCalibur, USA) within 1 h after staining.

TUNEL staining

Apoptotic NRK-52E cells were detected using the Terminal Deoxynucleotidyl Transferase (TdT)-Mediated dUTP Nick End Labeling (TUNEL) Apoptosis Detection Kit from Beyotime in Shanghai, China. In brief, NRK-52E cells were fixed with 4 % paraformaldehyde for 30 min, followed by a single wash with PBS. The cells were then treated with 0.3 % Triton X-100 (Beyotime) for 5 min. After two washes with PBS, the cells were exposed to 50 µl of TdT incubation buffer for 1.5 h at 37 °C in the dark. Following this, the cells were washed three times with PBS, and DAPI from Beyotime in Shanghai, China, was utilized to stain the cell nuclei. The results were observed using a fluorescent inverted microscope.

Animal experiments

Male C57BL/6 mice, 8 weeks old and weighing between 24-29 g, were obtained from Shanghai SLAC Laboratory Animal Co., Ltd. (Shanghai, China). The mice were housed under standard laboratory conditions with ad libitum access to rodent food and clean water, maintaining a normal circadian rhythm. The mice were randomly divided into four groups, each consisting of five mice: sham, unilateral ureteral occlusion (UUO), UUO + inhibitor NC, and UUO + miR-92a-3p inhibitor groups. The UUO model was induced using an established procedure [22]. Briefly, the mice were anesthetized with intraperitoneal pentobarbital sodium (40 mg/kg). An abdominal midline laparotomy was performed to expose the left ureter. Subsequently, the left ureter was obstructed using 2-point ligations with 4.0 silk, and the incision was closed in layers. For the sham group, the same abdominal midline laparotomy was performed, but the left ureter was not obstructed. The mice in the UUO + miR-92a-3p inhibitor group received daily subcutaneous injections of miR-92a-3p inhibitor (50 nM, GenePharma Corporation) through the tail vein, following a previously described protocol [23]. After 4 weeks, all mice were euthanized by cervical dislocation, and their renal tissues were collected for further experiments. Animal experiments were conducted according to the Guidelines for the Care and Use of Laboratory Animals at The Hai-nan Affiliated Hospital of Hainan Medical University and approved by the ethics committee of Hai-nan Affiliated Hospital of Hainan Medical University (No. HUA-A7D, Hainan, China).

Histopathological analysis

The collected renal tissues from various experimental groups were fixed in 10 % neutral buffered formalin, followed by paraffin embedding and slicing into 5-µm-thick sections. Hematoxylin and eosin (H&E) staining was performed on these renal sections using an H&E staining kit (Boster Biological Technology Co. Ltd, Wuhan, China). The staining process involved deparaffinizing, rehydrating, and staining the sections at room temperature, as per the manufacturer's instructions. In addition, Masson's trichrome staining was carried out on these sections using a modified Masson's Trichrome stain kit from Sigma-Aldrich, following the recommended protocols. Random interstitial cortical regions in the stained sections were then examined under an optical microscope (DSX100, Olympus Optical, Tokyo, Japan) to assess and analyze the histological changes in the kidney tissues. For immunohistochemistry (IHC), the renal sections were subjected to dewaxing, rehydration, and antigen retrieval by heating in boiling antigen unmasking solution. To block endogenous peroxidase activity, the sections were treated with 3 % H_2O_2. Subsequently, the kidney tissue sections were blocked with 5 % goat serum for 1 h and then incubated overnight at 4 °C with the primary antibody against α-SMA (1:1000, Abcam, Cambridge, UK). For detection of rabbit primary antibody, a biotinylated mouse anti-rabbit secondary antibody was utilized. The sections were then stained with DAB solution (ZSGB-BIO, Beijing, China) for

visualization. Images were acquired using the Leica DM 1000 microscope image system. Masson staining and immunostaining intensity were evaluated using the following scoring criteria: high-power fields (×200 magnification) were randomly chosen and photographed for each group. Scores were assigned based on the degree and extent of tubular degeneration and necrosis, tubular atrophy, inflammatory cell infiltration, and fibrosis. The involvement was classified and scored as none (0), mild (1), moderate (2), or severe (3) [24]. The extent of the lesion was determined by calculating the blue area of collagen from Masson staining. The stained area was quantified based on the average optical density in the immunostaining intensity scores.

Table 1. Primers for quantitative real-time PCR.

Target Gene	Forward (5' - 3')	Reverse (5' - 3')
miR-92a-3p	ATTGCACTTGTCCCGGCC	GAACATGTCTGCGTATCTC
LIN28A	CATGGGCTCGGTGTCCAAC	CCTCCTTGAGGCTTCGGAAC
Inos	GCCCAGCCAGCCCAAC	GCAGCTTGTCCAGGGATTCT
IL-6	CAACGATGATGCACTTGCAGA	TGTGACTCCAGCTTATCTCTTGG
TNF	ACTGAACTTCGGGGTGATCG	GATAGCAAATCGGCTGACGG
U6	GCATGACGTCTGCTTTGGA	CCACAATCATTCTGCCATCA
GAPDH	TGGTGAAGGTCGGTGTGAAC	TTCCCATTCTCGGCCTTGAC

Abbreviations. Inos, inducible nitric oxide synthase; TNF, tumor necrosis factor.

Western blot analysis

Whole-protein extracts from cells and renal tissues were prepared by scraping the cells or from renal tissues by homogenization, using RIPA lysis buffer from Beyotime in Shanghai, China. After centrifugation at 16000× g for 10 min at 4 °C, the supernatants were collected for protein quantification using a BCA kit (Beyotime). For protein analysis, electrophoresis was performed, and the proteins were transferred to polyvinylidene difluoride (PVDF) membranes from Bio-Rad. The blots were then blocked with 5 % (m/v) BSA in Tris-buffered saline buffer-Tween (TBS-T, Cell Signaling Technology) and incubated with primary antibodies against iNOS (1:500, ab3523, Abcam), LIN28A (1:1000, ab175352, Abcam), Bcl-2 (1:1000, ab16904, Abcam), cleaved caspase-3 (1:5000, ab214430, Abcam), α-SMA (1:1000, 19245, Cell Signaling Technology), and GAPDH (1:10000, ab181602, Abcam) at 4 °C overnight. After washing with TBS-T, the membranes were incubated with a horseradish peroxi-dase-conjugated secondary antibody for 2 h. The protein bands were visualized using the hypersensitive electrochemil-uminescence (ECL) kit (Thermo Fisher Scientific, Inc.).

Statistical analysis

All experimental data were obtained in triplicates to ensure reproducibility. Statistical analysis was performed using GraphPad Prism 8.0 software (GraphPad Software, Inc., La Jolla, CA, USA). Data were expressed as mean ± standard deviation (SD). Statistical comparisons between two groups were conducted using the Student's *t*-test, while for comparisons involving more than two groups, one-way ANOVA followed by Tukey's *post hoc* test was applied. A $p<0.05$ was considered statistically significant.

Ethics approval and consent to participate

The study is in accordance with the Declaration of Helsinki, all methods are reported in accordance with ARRIVE guidelines (https://arriveguidelines.org) for the reporting of animal experiments, and all experimental protocols were approved by the ethics committee of Hainan Affiliated Hospital of Hainan Medical University (No. HUA-A7D, Hainan, China). Informed consent is not applicable. All methods were carried out in accordance with relevant guidelines and regulations.

Results

MiR-92a-3p enhanced LPS-induced M1 macrophage polarization

To investigate the functional role of miR-92a-3p in the polarization of M1 macrophages, we transfected miR-

92a-3p mimics and mimics NC into RAW264.7 cells that were induced with LPS. As shown in Figure 1A, the expression of miR-92a-3p was significantly increased in RAW264.7 cells transfected with miR-92a-3p mimics compared to the NC group. Next, we examined the markers of M1 macrophages and inflammation. We found that the mRNA levels of IL-6, Inos, and TNF (Fig. 1B) as well as the protein level of iNOS (Fig. 1C) were notably elevated in LPS-stimulated RAW264.7 cells, and this effect was further enhanced after overexpressing miR-92a-3p. ELISA assay results demonstrated that miR-92a-3p overexpression promoted a further increase in IL-6 and TNF-α production in LPS-stimulated RAW264.7 cells (Fig. 1D). Conversely, when we transfected miR-92a-3p inhibitor into RAW264.7 cells, the expression of miR-92a-3p was reduced (Fig. 1E). As a result, the elevated expression levels of IL-6, Inos, and TNF mRNA (Fig. 1F) as well as iNOS protein (Fig. 1G) in RAW264.7-derived M1 macrophages were significantly reversed. Moreover, the knockdown of miR-92a-3p noticeably attenuated the increased concentration of IL-6 and TNF-α in LPS-stimulated RAW264.7 cells (Fig. 1H). Our findings suggest that miR-92a-3p plays a crucial role in promoting the polarization of M1 macrophages and the associated inflammatory response.

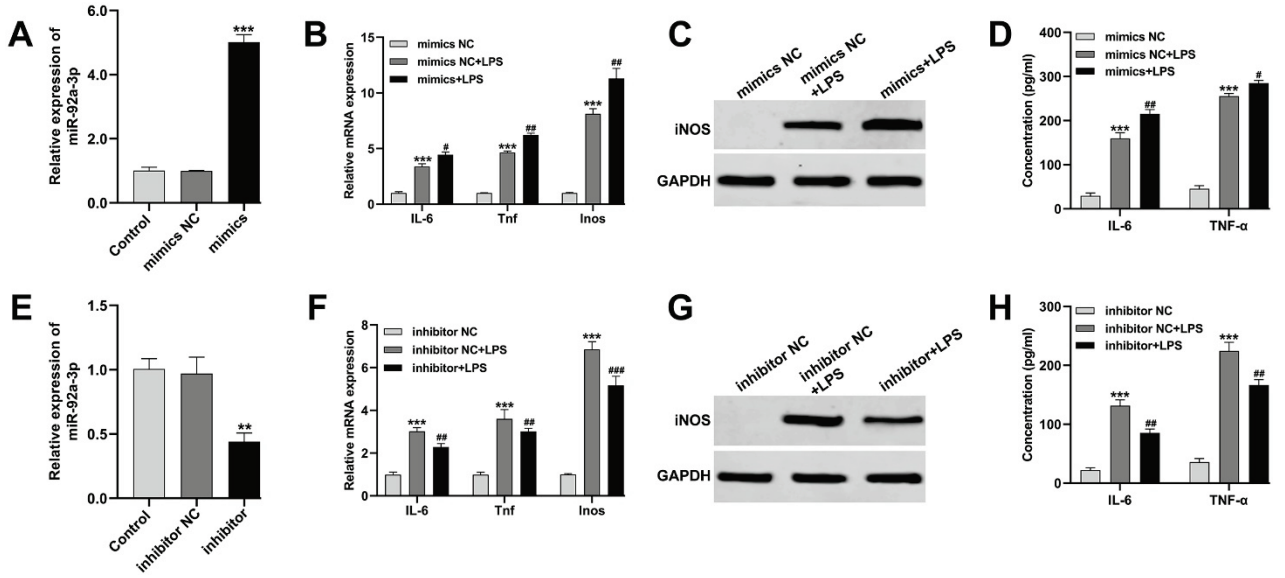

Fig. 1. MiR-92a-3p enhanced LPS-induced M1 macrophage polarization. (**A**) The expression of miR-92a-3p was detected by quantitative real time PCR in RAW264.7 cells transfected with miR-92a-3p mimics or mimics NC. (**B**) The mRNA expression level of IL-6, Inos, and TNF was detected in RAW264.7 cells transfected with miR-92a-3p mimics or mimics NC. (**C**) The protein expression level of iNOS was validated by western blot analysis in RAW264.7 cells transfected with miR-92a-3p mimics or mimics NC. (**D**) The concentration levels of IL-6 and TNF-α were exhibited by ELISA in LPS-activated RAW264.7 cells transfected with miR-92a-3p mimics or mimics NC. (**E**) The expression of miR-92a-3p was detected by quantitative real time PCR in RAW264.7 cells transfected with miR-92a-3p inhibitor or inhibitor NC. (**F**) The mRNA expression level of IL-6, Inos, and TNF was detected in RAW264.7 cells transfected with miR-92a-3p inhibitor or inhibitor NC. (**G**) The protein expression level of iNOS was validated by western blot analysis in RAW264.7 cells transfected with miR-92a-3p inhibitor or inhibitor NC. (**H**) The concentration levels of IL-6 and TNF-α were exhibited by ELISA in LPS-activated RAW264.7 cells transfected with inhibitor or inhibitor NC. Data were expressed as mean ± SD. ** $p<0.01$, *** $p<0.001$, compared with mimics NC or inhibitor NC; # $p<0.05$, ## $p<0.01$, ### $p<0.001$, compared with mimics NC + LPS or inhibitor NC + LPS.

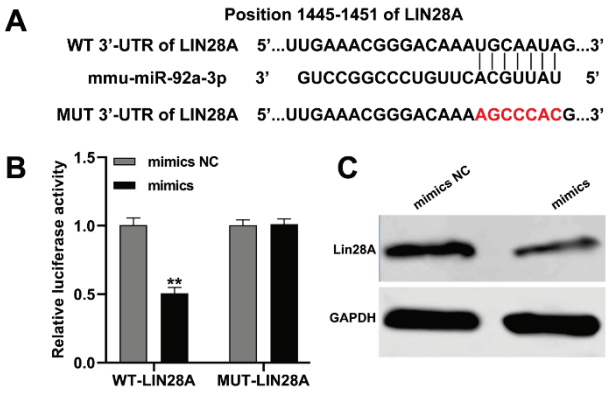

Fig. 2. LIN28A was a direct target gene of miR-92a-3p. (**A**) The binding region between LIN28A mRNA 3′-UTR and miR-92a-3p in wild- and mutant-type plasmids. (**B**) LIN28A transcriptional activity in 293T cells transfected with miR-92a-3p mimics or mimics NC was detected by the luciferase reporter gene assay system. (**C**) The protein expression of LIN28A was determined using western blot analysis in RAW264.7 cells transfected with miR-92a-3p mimics or mimics NC. Data were expressed as mean ± SD. ** $p<0.01$, compared with mimics NC.

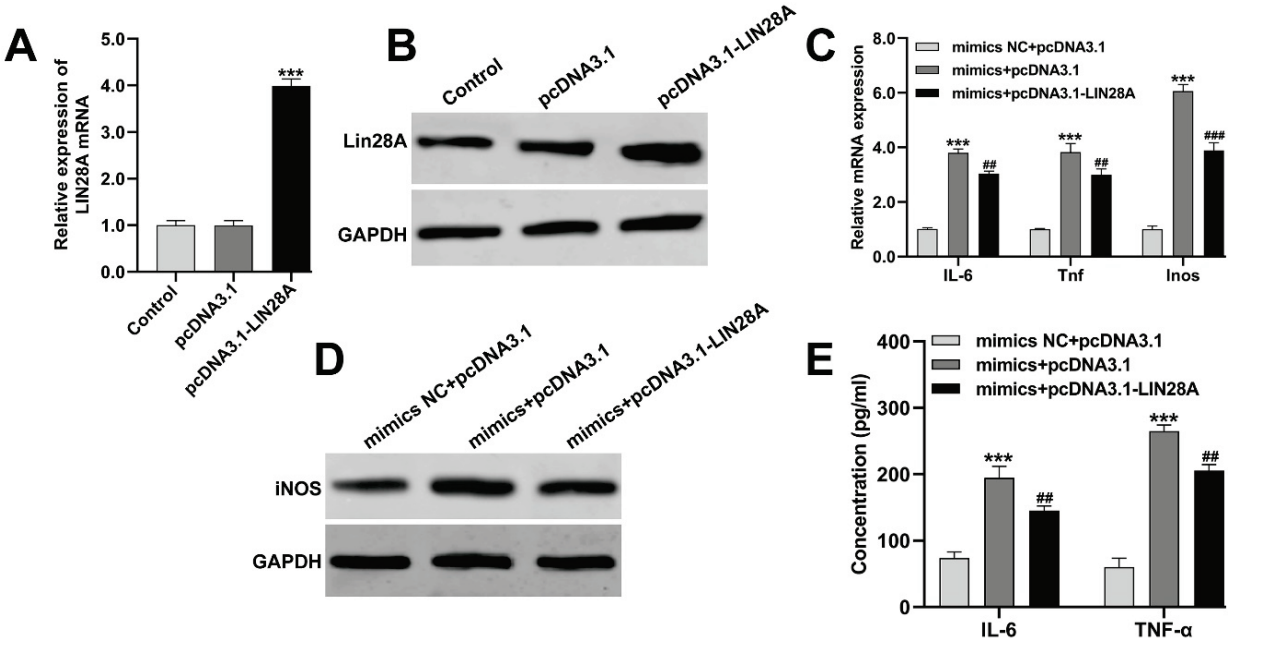

Fig. 3. LIN28A overexpression reversed the promotive effects of miR-92a-3p on LPS-induced M1 macrophage polarization. (**A-B**) The expression levels of LIN28A mRNA and protein were determined by quantitative real time PCR and western blot analysis in RAW264.7 cells transfected with pcDNA3.1-LIN28A or pcDNA3.1. Co-transfection using miR-92a-3p mimics and pcDNA3.1-LIN28A was performed in RAW264.7 cells stimulated with LPS. *** $p<0.001$, compared with pcDNA3.1; (**C**) The mRNA expression level of IL-6, Inos, and TNF was detected in co-transfected RAW264.7 cells. (**D**) The protein expression level of iNOS was validated by western blot analysis in co-transfected RAW264.7 cells. (**E**) The concentration levels of IL-6 and TNF-α were measured by ELISA in co-transfected RAW264.7 cells. Data were expressed as mean ± SD. *** $p<0.001$, compared with mimics NC + pcDNA3.1; ## $p<0.01$, ### $p<0.001$, compared with mimics + pcDNA3.1.

LIN28A was a direct target gene of miR-92a-3p

Based on predictions from the TargetScan database, a specific binding site was identified between miR-92a-3p and the 3′-UTR of LIN28A mRNA (Fig. 2A), suggesting that LIN28A might be a direct target of miR-92a-3p. To experimentally verify this direct binding, plasmids containing wild-type and mutant-type LIN28A mRNA 3′-UTR were constructed, and a dual-luciferase reporter assay was performed. The results demonstrated that miR-92a-3p significantly inhibited the luciferase activity of the wild-type LIN28A plasmid containing the 3′-UTR, while the mutant-type LIN28A plasmid remained unaffected (Fig. 2B). Furthermore, to validate the downregulation of LIN28A by miR-92a-3p, Western blot analysis was conducted in RAW264.7 cells transfected with miR-92a-3p mimics. The protein levels of LIN28A were found to be significantly reduced in RAW264.7 cells expressing miR-92a-3p mimics compared to the mimics NC group (Fig. 2C). These experimental results provide confirmation that miR-92a-3p directly targets LIN28A by binding to its 3′-UTR through base complementary pairing.

LIN28A overexpression reversed the promotive effects of miR-92a-3p on LPS-induced M1 macrophage polarization

To further investigate whether LIN28A acts as a downstream regulator in miR-92a-3p-mediated regulation of LPS-induced M1 macrophage polarization, rescue experiments were conducted in RAW264.7 cells stimulated with LPS. Co-transfection was performed using miR-92a-3p mimics and pcDNA3.1-LIN28A. Initially, we confirmed that the expression levels of LIN28A mRNA (Fig. 3A) and protein (Fig. 3B) were significantly increased in RAW264.7 cells transfected with pcDNA3.1-LIN28A compared to those transfected with pcDNA3.1 alone. Next, we assessed the impact of LIN28A overexpression on the promotive effects induced by miR-92a-3p mimics. The increased expression of IL-6, Inos, and TNF mRNA (Fig. 3C), as well as the protein level of iNOS (Fig. 3D) induced by miR-92a-3p mimics, were all notably abolished after LIN28A overexpression in LPS-stimulated RAW264.7 cells. Furthermore, ELISA assay results demonstrated that LIN28A overexpression significantly suppressed the elevated levels of IL-6 and TNF-α in LPS-stimulated RAW264.7 cells (Fig. 3E). Collectively, these findings indicate that overexpressed LIN28A effectively reverses the promotive effects of miR-92a-3p mimics on M1 macrophage polarization.

MiR-92a-3p in RAW264.7 cells augmented the apoptotic rate of LPS-stimulated NRK-52E cells by targeting LIN28A

To assess the impact of M1 macrophage polarization on renal injury *in vivo*, co-culture experiments were conducted using LPS-stimulated NRK-52E cells and RAW264.7 cells co-overexpressing miR-92a-3p and LIN28A. The aim was to explore how the miR-92a-3p/LIN28A axis in RAW264.7 cells influenced the apoptosis status of NRK-52E cells. Flow cytometry assay (Fig. 4A) and TUNEL staining (Fig. 4B) were performed to analyze the apoptosis status of NRK-52E cells. Upon LPS treatment, the early and late apoptotic percentages of NRK-52E cells were higher compared to the control group. Co-culture with RAW264.7 cells overexpressing miR-92a-3p significantly elevated the early and late apoptotic percentages of NRK-52E cells, indicating that miR-92a-3p accelerated RAW264.7-induced apoptosis. However, overexpression of LIN28A in RAW264.7 cells inhibited the increased apoptotic level of NRK-52E cells induced by miR-92a-3p. Furthermore, western blot analysis (Fig. 4C) revealed that LPS treatment led to a significant downregulation of Bcl-2 and upregulation of cleaved caspase-3 protein expression in NRK-52E cells. Co-culture with RAW264.7 cells slightly enhanced the expression of these proteins. Importantly, miR-92a-3p induced a significant decrease in Bcl-2 expression and an increase in cleaved caspase-3 expression, both of which were attenuated when RAW264.7 cells overexpressed LIN28A. These findings further indicate that M1 polarization of RAW264.7 cells could accelerate the apoptosis of NRK-52E cells. Additionally, the overexpression of miR-92a-3p can further accelerate NRK-52E cell apoptosis by promoting M1 macrophage activation *via* targeting LIN28A.

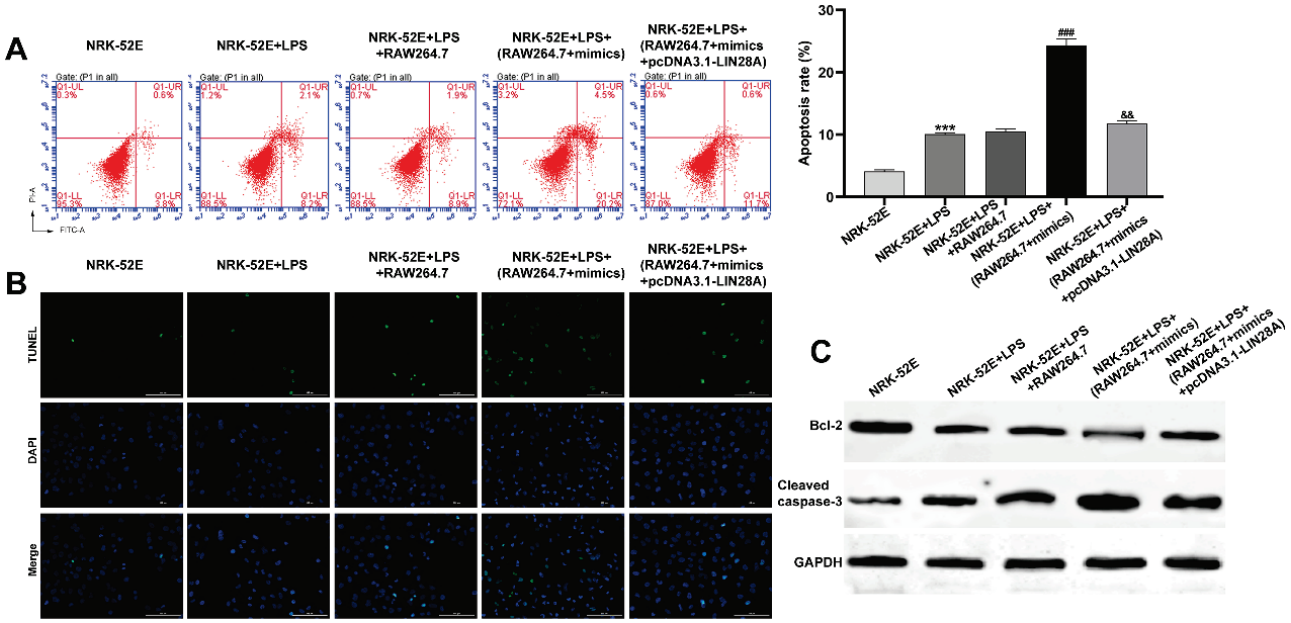

Fig. 4. MiR-92a-3p in RAW264.7 cells augmented the apoptotic rate of LPS-stimulated NRK-52E cells by targeting LIN28A. Co-culture experiments were conducted using LPS-stimulated NRK-52E cells and RAW264.7 cells co-overexpressing miR-92a-3p and LIN28A. (**A**) The apoptotic ratio of NRK-52E cells from co-culture system, induced by LPS were detected *via* flow cytometer. (**B**) Apoptotic NRK-52E cells from co-culture system, induced by LPS were detected using TUNEL staining. (**C**) The Bcl-2 and cleaved-caspase-3 protein levels in NRK-52E cells from co-culture system, induced by LPS were analyzed using western blot analysis. Data were expressed as mean ± SD. *** $p<0.001$, compared with NRK-52E; ### $p<0.001$, compared with NRK-52E + LPS + RAW264.7; && $p<0.01$, compared with NRK-52E + LPS + (RAW264.7 + mimics).

In vivo inhibition of miR-92a-3p ameliorated renal fibrosis and M1 macrophage activation

Next, we aimed to investigate the impact of miR-92a-3p on the M1 macrophage activation in UUO-induced obstructive renal fibrosis using an *in vivo* mouse model. As shown in Figure 5A, H&E staining revealed that mice in the sham group had normal glomeruli and tubules, while those in the UUO group exhibited various pathological changes, such as renal interstitial edema, epithelial cell necrosis, tubular dilatation, and infiltration of lymphocytes and monocytes in the interstitial space. Remarkably, administration of a miR-92a-3p inhibitor visibly improved these pathological changes in the UUO group. Additionally, Masson's trichrome staining of renal sections from

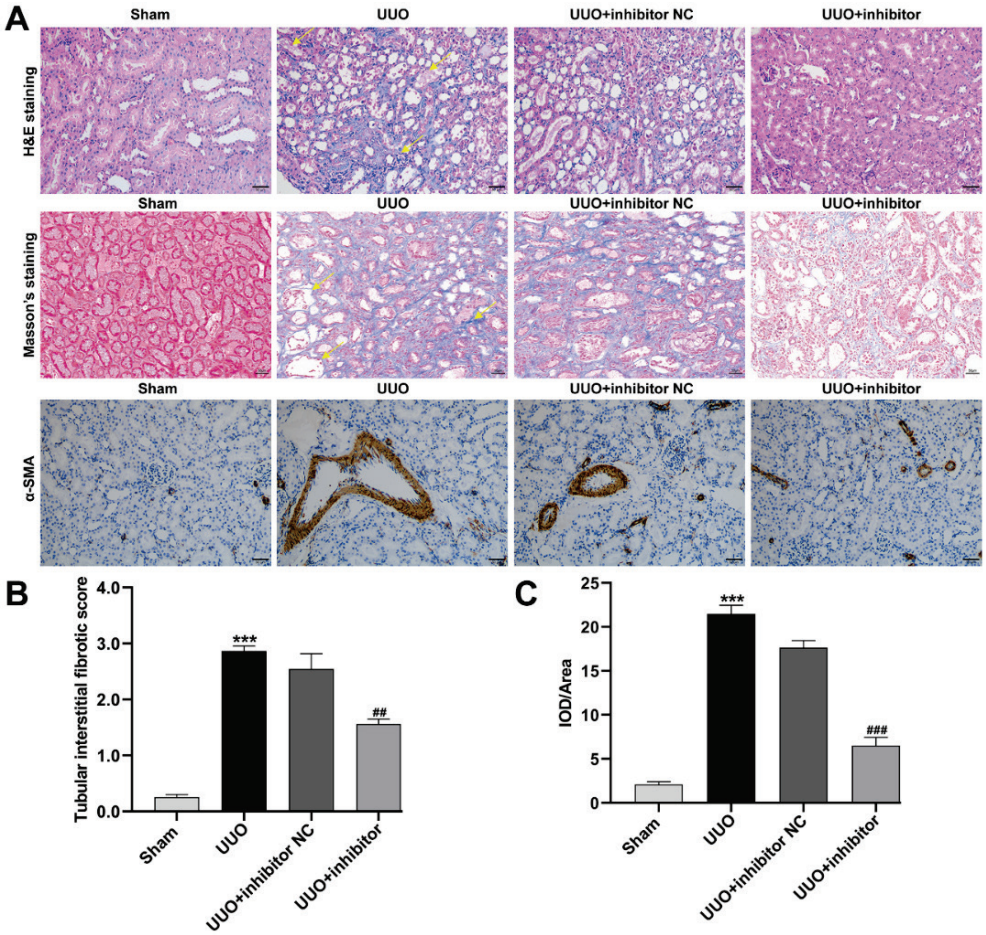

Fig. 5. *In vivo* inhibition of miR-92a-3p ameliorated renal fibrosis. Male C57BL/6 mice underwent UUO surgery, followed by received daily subcutaneous injections of miR-92a-3p inhibitor (50 nM) through the tail vein. (**A**) Representative micrographs of hematoxylin and eosin (H&E) and Masson's staining demonstrate kidney injury in indicated group; immunohistochemical staining of α-SMA protein in kidney tissue; (**B**) quantification of renal tubular interstitial fibrotic score (**C**) compared with the NC-treated-UUO group, the expression of α-SMA decreased in the UUO kidneys of miR-92a-3p knockout mice. n=5. *** $p<0.001$, compared with sham; ## $p<0.01$, ### $p<0.001$, compared with UUO + inhibitor NC.

UUO mice showed increased renal interstitial fibrosis, characterized by an augmented stromal area, extracellular matrix accumulation, and extensive blue stained fibers. However, treatment with the miR-92a-3p inhibitor ameliorated these fibrotic changes (Fig. 5A-B). Furthermore, our IHC results indicated that the significantly elevated renal fibrosis marker α-SMA in the UUO group, compared with the sham group, was notably attenuated after treatment with the miR-92a-3p inhibitor (Fig. 5A-C). Subsequently, we confirmed the downregulation of miR-92a-3p in the UUO group following the administration of the miR-92a-3p inhibitor (Fig. 6A). We then proceeded to analyze the effect of miR-92a-3p on M1 macrophage activation-related molecules. Western blot analysis demonstrated a significant increase in LIN28A expression but a notable reduction in iNOS and α-SMA expression levels in renal samples from the UUO-induced mouse model after inhibition of miR-92a-3p (Fig. 6B). Similarly, the miR-92a-3p inhibitor led to reduced expression of pro-inflammatory cytokines (IL-6 and TNF) in UUO mice, as assessed by quantitative real-time PCR (Fig. 6C-D) and ELISA assay (Fig. 6E-F). Taken together, these findings provide compelling evidence that miR-92a-3p plays a crucial role in reducing UUO-induced obstructive renal fibrosis and M1 macrophage activation.

Discussion

Numerous studies have provided substantial support for the role of M1 macrophages in promoting kidney injury and fibrosis [25-27]. In our research, we focused on elucidating the specific role of M1 macrophages in kidney inflammation and fibrosis, considering the ongoing debate about the role of M2 macrophages in this context [28]. Our study presents initial evidence indicating that miR-92a-3p promotes M1 macrophage polarization and inflammation in

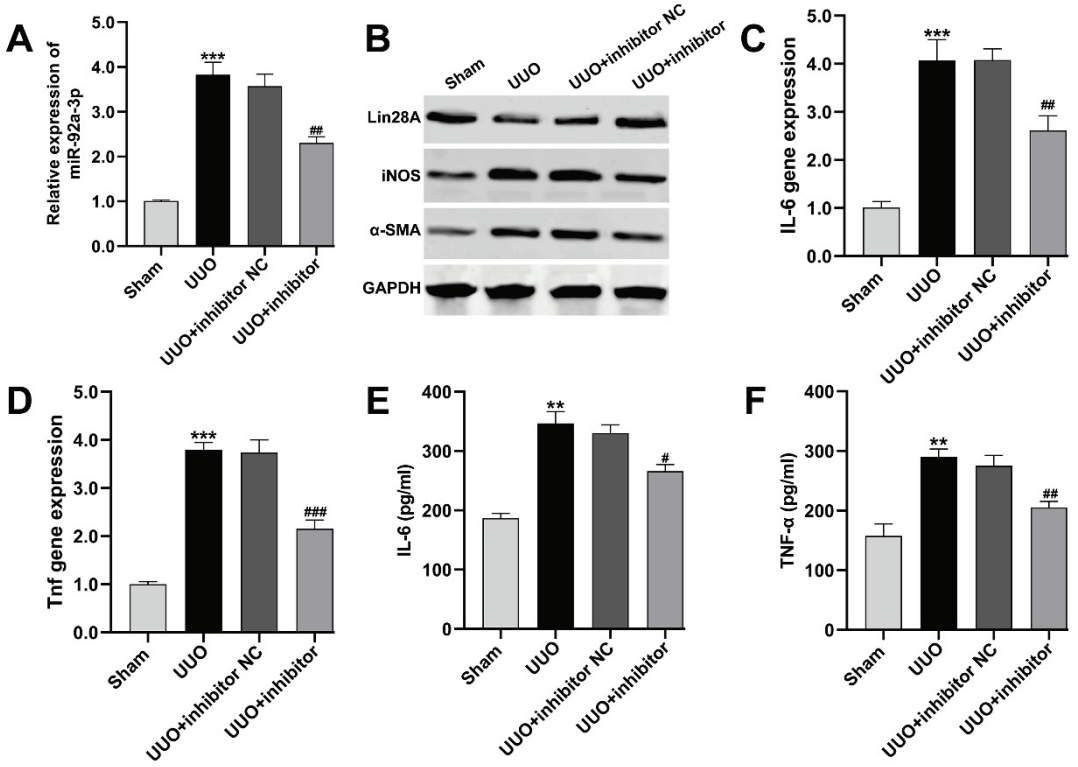

Fig. 6. *In vivo* inhibition of miR-92a-3p ameliorated M1 macrophage activation. Male C57BL/6 mice underwent UUO surgery, followed by received daily subcutaneous injections of miR-92a-3p inhibitor (50 nM) through the tail vein. (**A**) The expression of miR-92a-3p was detected by quantitative real time PCR in the renal samples. (**B**) Western blotting of LIN28A, iNOS and α-SMA in renal tissues. (**C-D**) The mRNA expression levels of IL6 and TNF were determined using quantitative real time PCR. (**E-F**) The concentration levels of IL-6 and TNF-α were measured by ELISA in renal samples. Data were expressed as mean ± SD. n=5. ** $p<0.01$, *** $p<0.001$, compared with sham; $^{\#}p<0.05$, $^{\#\#}p<0.01$, $^{\#\#\#}p<0.001$, compared with UUO + inhibitor NC.

LPS-stimulated RAW264.7 cells. One the one hand, dysregulated miR-92a-3p expression has been implicated in various inflammation-related diseases. For example, miR-92a-3p is involved in regulating the expression of ADAMTS-4/5, which may contribute to osteoarthritis (OA) development [29]. Additionally, inhibiting miR-92a-3p in human coronary artery endothelial cells has shown promise in reducing renal injury-induced atherosclerosis [14]. Shen *et al.* [30] have reported its involvement in cigarette smoke extract (CSE)-induced hyperinflammation in chronic obstructive pulmonary disease (COPD). Moreover, miR-92a-3p exacerbates intrapulmonary inflammation, pulmonary injury, and dysfunction in LPS-induced acute lung injury [31]. On the other hand, miR-92a-3p found in alveolar epithelial cell (AEC) exosomes has been shown to mediate alveolar macrophage activation in sepsis-induced acute lung injury [32]. Furthermore, miR-92a-3p stimulates the secretion of proinflammatory cytokine IL-6 from tumor-associated macrophages *via* a TLR7/8-dependent mechanism, promoting liposarcoma cell proliferation, invasion, and metastasis [33]. These biochemical and molecular findings suggest that miR-92a-3p may play an activating role in the progression of CKD by enhancing LPS-induced inflammation and M1 macrophage polarization.

The TargetScan database identified LIN28A as a potential target of miR-92a-3p, leading us to hypothesize that LIN28A is indeed the target gene of miR-92a-3p. Through luciferase activity assays, we confirmed that miR-92a-3p targets and downregulates LIN28A, representing a crucial step in an unknown mechanism of CKD progression. Our findings revealed that miR-92a-3p promotes M1 macrophage polarization and inflammation in LPS-stimulated RAW264.7 cells. To elucidate the functional significance of miR-92a-3p targeting LIN28A, we performed rescue experiments, which demonstrated that LIN28A overexpression not only reversed the promotive effects of miR-92a-3p on LPS-induced inflammation and M1 macrophage polarization but also attenuated the increased apoptotic rate induced by miR-92a-3p in LPS-stimulated NRK-52E cells. Importantly, our findings align with previous studies on LIN28A as an RNA-binding protein that enhances glucose uptake and insulin sensitivity, suggesting its potential as a therapeutic target for patients with diabetic cardiomyopathy (DCM) [34,35]. LIN28A

has also been reported to inhibit cardiomyocyte apoptosis by enhancing mitochondrial biogenesis and function under high glucose/high-fat conditions [36]. Moreover, *in vitro* and *in vivo* studies have shown that LIN28A overexpression can protect pancreatic β-cells from β-cell destruction induced by streptozotocin (STZ) [37]. In the context of kidney cells, Jung *et al.* [20] reported reduced LIN28A expression in TGF-β1-stimulated HK-2 cells and demonstrated its potential to attenuate renal fibrosis in obstructive nephropathy, suggesting LIN28A as a potential therapeutic target for CKD. Furthermore, LIN28A has been shown to have regulatory effects on glycolytic metabolism in human embryonic kidney cells [19] and on high glucose-induced renal tubular epithelial injury [38]. However, we acknowledge a limitation of the present study, as we did not directly examine the regulatory role of LIN28A alone in LPS-stimulated RAW264.7 cells and NRK-52E cells, which could have strengthened our conclusions.

Remarkably, our study revealed that inhibiting miR-92a-3p exerts anti-fibrosis and anti-inflammatory effects in UUO models of kidney disease. At the molecular level, we demonstrated that miR-92a-3p inhibition led to a reduction in the expression of LIN28A, as well as renal fibrosis marker α-SMA, M1 macrophage marker iNOS, and pro-inflammatory cytokines (IL-6 and TNF) in renal samples from UUO mice. Consistent with our findings, miR-92a-3p has been identified as one of the fibrosis-related miRNAs involved in the development of fibrotic lesions in the lungs of post-COVID-19 patients [39]. Furthermore, serum levels of miR-92a-3p have shown potential as a diagnostic marker for distinguishing Filipino schistosomiasis japonica subjects with fibrosis grades I-III from those without fibrosis [40]. Mechanistically, mmu-miR-92a-3p has been found to regulate pulmonary fibrosis by modulating the Cpeb4-mediated Smad2/3 signaling pathway [41]. It is well-established that excessive and prolonged inflammation plays a critical role in driving fibrosis [42,43]. M1 macrophages, characterized by their secretion of pro-inflammatory cytokines and chemokines, are actively involved in immune responses and immune surveillance [44]. Over-activation of M1 macrophages has been implicated in the pathogenesis of various inflammatory, autoimmune, and chronic diseases [45,46]. Building upon these findings, our study provides compelling evidence that miR-92a-3p serves as a crucial regulator of kidney inflammation and fibrosis by enhancing LPS-induced M1 macrophage polarization.

In summary, our study has elucidated the significance of miR-92a-3p/LIN28A signaling in the control of LPS-induced M1 macrophage polarization and UUO-induced obstructive renal fibrosis. Our findings provide evidence that miR-92a-3p plays a promotive role in renal inflammation and fibrosis by enhancing M1 macrophage polarization through the targeting of LIN28A. The regulatory network involving the miR-92a-3p/LIN28A axis sheds light on a better understanding of the potential mechanisms underlying the pathogenesis and progression of CKD.

Conflict of Interest

There is no conflict of interest.

Acknowledgements

This work is supported by Natural Science Foundation of Hainan Province (NO. 822MS169).

References

1. Jha V, Garcia-Garcia G, Iseki K, Li Z, Naicker S, Plattner B, Saran R, ET AL. Chronic kidney disease: global dimension and perspectives. Lancet 2013;382:260-272. https://doi.org/10.1016/S0140-6736(13)60687-X
2. Adair KE, Bowden RG. Ameliorating Chronic Kidney Disease Using a Whole Food Plant-Based Diet. Nutrients 2020;12:1007. https://doi.org/10.3390/nu12041007
3. Harris RC, Neilson EG. Toward a unified theory of renal progression. Annu Rev Med 2006;57:365-380. https://doi.org/10.1146/annurev.med.57.121304.131342
4. Wang Y, Harris DC. Macrophages in renal disease. J Am Soc Nephrol 2011;22:21-27. https://doi.org/10.1681/ASN.2010030269
5. Tang PM, Nikolic-Paterson DJ, Lan HY. Macrophages: versatile players in renal inflammation and fibrosis. Nat Rev Nephrol 2019;15:144-158. https://doi.org/10.1038/s41581-019-0110-2
6. Ruytinx P, Proost P, Van Damme J, Struyf S. Chemokine-Induced Macrophage Polarization in Inflammatory Conditions. Front Immunol 2018;9:1930. https://doi.org/10.3389/fimmu.2018.01930

7. Gordon S, Martinez FO. Alternative activation of macrophages: mechanism and functions. Immunity 2010;32:593-604. https://doi.org/10.1016/j.immuni.2010.05.007
8. Bartel DP. MicroRNAs: genomics, biogenesis, mechanism, and function. Cell 2004;116:281-297. https://doi.org/10.1016/S0092-8674(04)00045-5
9. Ha M, Kim VN. Regulation of microRNA biogenesis. Nat Rev Mol Cell Biol 2014;15:509-524. https://doi.org/10.1038/nrm3838
10. Ding C, Zheng J, Wang B, Li Y, Xiang H, Dou M, Qiao Y, ET AL. Exosomal MicroRNA-374b-5p From Tubular Epithelial Cells Promoted M1 Macrophages Activation and Worsened Renal Ischemia/Reperfusion Injury. Front Cell Dev Biol 2020;8:587693. https://doi.org/10.3389/fcell.2020.587693
11. Hao X, Luan J, Jiao C, Ma C, Feng Z, Zhu L, Zhang Y, ET AL. LNA-anti-miR-150 alleviates renal interstitial fibrosis by reducing pro-inflammatory M1/M2 macrophage polarization. Front Immunol 2022;13:913007. https://doi.org/10.3389/fimmu.2022.913007
12. Cun J, Yang Q. Bioinformatics-based interaction analysis of miR-92a-3p and key genes in tamoxifen-resistant breast cancer cells. Biomed Pharmacother 2018;107:117-128. https://doi.org/10.1016/j.biopha.2018.07.158
13. Wang R, Zhao H, Zhang Y, Zhu H, Su Q, Qi H, Deng J, Xiao C. Identification of MicroRNA-92a-3p as an Essential Regulator of Tubular Epithelial Cell Pyroptosis by Targeting Nrf1 via HO-1. Front Genet 2020;11:616947. https://doi.org/10.3389/fgene.2020.616947
14. Wiese CB, Zhong J, Xu ZQ, Zhang Y, Ramirez Solano MA, Zhu W, Linton MF, ET AL. Dual inhibition of endothelial miR-92a-3p and miR-489-3p reduces renal injury-associated atherosclerosis. Atherosclerosis 2019;282:121-131. https://doi.org/10.1016/j.atherosclerosis.2019.01.023
15. Piskounova E, Polytarchou C, Thornton JE, LaPierre RJ, Pothoulakis C, Hagan JP, Iliopoulos D, Gregory RI. Lin28A and Lin28B inhibit let-7 microRNA biogenesis by distinct mechanisms. Cell 2011;147:1066-1079. https://doi.org/10.1016/j.cell.2011.10.039
16. Xu B, Zhang K, Huang Y. Lin28 modulates cell growth and associates with a subset of cell cycle regulator mRNAs in mouse embryonic stem cells. RNA 2009;15:357-361. https://doi.org/10.1261/rna.1368009
17. Polesskaya A, Cuvellier S, Naguibneva I, Duquet A, Moss EG, Harel-Bellan A. Lin-28 binds IGF-2 mRNA and participates in skeletal myogenesis by increasing translation efficiency. Genes Dev 2007;21:1125-1138. https://doi.org/10.1101/gad.415007
18. Zhu H, Shyh-Chang N, Segre AV, Shinoda G, Shah SP, Einhorn WS, Takeuchi A, ET AL. The Lin28/let-7 axis regulates glucose metabolism. Cell 2011;147:81-94. https://doi.org/10.1016/j.cell.2011.08.033
19. Docherty CK, Salt IP, Mercer JR. Lin28A induces energetic switching to glycolytic metabolism in human embryonic kidney cells. Stem Cell Res Ther 2016;7:78. https://doi.org/10.1186/s13287-016-0323-2
20. Jung GS, Hwang YJ, Choi JH, Lee KM. Lin28a attenuates TGF-β-induced renal fibrosis. BMB Rep 2020;53:594-599. https://doi.org/10.5483/BMBRep.2020.53.11.153
21. Guo L, Cheng X, Chen H, Chen C, Xie S, Zhao M, Liu D, ET AL. Induction of breast cancer stem cells by M1 macrophages through Lin-28B-let-7-HMGA2 axis. Cancer Lett 2019;452:213-225. https://doi.org/10.1016/j.canlet.2019.03.032
22. Ding H, Xu Y, Jiang N. Upregulation of miR-101a Suppresses Chronic Renal Fibrosis by Regulating KDM3A via Blockade of the YAP-TGF-beta-Smad Signaling Pathway. Mol Ther Nucleic Acids 2020;19:1276-1289. https://doi.org/10.1016/j.omtn.2020.01.002
23. Krutzfeldt J, Rajewsky N, Braich R, Rajeev KG, Tuschl T, Manoharan M, Stoffel M. Silencing of microRNAs in vivo with 'antagomirs'. Nature 2005;438:685-689. https://doi.org/10.1038/nature04303
24. Kikuchi H, Katsuramaki T, Kukita K, Taketani S, Meguro M, Nagayama M, Isobe M, Mizuguchi T, Hirata K. New strategy for the antifibrotic therapy with oral administration of FR260330 (a selective inducible nitric oxide synthase inhibitor) in rat experimental liver cirrhosis. Wound Repair Regen 2007;15:881-888. https://doi.org/10.1111/j.1524-475X.2007.00308.x
25. Huen SC, Cantley LG. Macrophage-mediated injury and repair after ischemic kidney injury. Pediatr Nephrol 2015;30:199-209. https://doi.org/10.1007/s00467-013-2726-y

26. Ko GJ, Boo CS, Jo SK, Cho WY, Kim HK. Macrophages contribute to the development of renal fibrosis following ischaemia/reperfusion-induced acute kidney injury. Nephrol Dial Transplant 2008;23:842-852. https://doi.org/10.1093/ndt/gfm694
27. Wen Y, Lu X, Ren J, Privratsky JR, Yang B, Rudemiller NP, Zhang J, ET AL. KLF4 in Macrophages Attenuates TNFalpha-Mediated Kidney Injury and Fibrosis. J Am Soc Nephrol 2019;30:1925-1938. https://doi.org/10.1681/ASN.2019020111
28. Anders HJ, Ryu M. Renal microenvironments and macrophage phenotypes determine progression or resolution of renal inflammation and fibrosis. Kidney Int 2011;80:915-925. https://doi.org/10.1038/ki.2011.217
29. Mao G, Wu P, Zhang Z, Zhang Z, Liao W, Li Y, Kang Y. MicroRNA-92a-3p Regulates Aggrecanase-1 and Aggrecanase-2 Expression in Chondrogenesis and IL-1beta-Induced Catabolism in Human Articular Chondrocytes. Cell Physiol Biochem 2017;44:38-52. https://doi.org/10.1159/000484579
30. Shen Y, Lu H, Song G. MiR-221-3p and miR-92a-3p enhances smoking-induced inflammation in COPD. J Clin Lab Anal 2021;35:e23857. https://doi.org/10.1002/jcla.23857
31. Wang C, Li YH, Yang ZT, Cheng NT, Tang HX, Xu M. The function and mechanism of microRNA-92a-3p in lipopolysaccharide-induced acute lung injury. Immunopharmacol Immunotoxicol 2022;44:47-57. https://doi.org/10.1080/08923973.2021.2001497
32. Liu F, Peng W, Chen J, Xu Z, Jiang R, Shao Q, Zhao N, Qian K. Exosomes Derived From Alveolar Epithelial Cells Promote Alveolar Macrophage Activation Mediated by miR-92a-3p in Sepsis-Induced Acute Lung Injury. Front Cell Infect Microbiol 2021;11:646546. https://doi.org/10.3389/fcimb.2021.646546
33. Casadei L, Calore F, Creighton CJ, Guescini M, Batte K, Iwenofu OH, Zewdu A, ET AL. Exosome-Derived miR-25-3p and miR-92a-3p Stimulate Liposarcoma Progression. Cancer Res 2017;77:3846-3856. https://doi.org/10.1158/0008-5472.CAN-16-2984
34. You P, Cheng Z, He X, Deng J, Diao J, Chen H, Cheng G. Lin28a protects against diabetic cardiomyopathy through Mst1 inhibition. J Cell Physiol 2020;235:4455-4465. https://doi.org/10.1002/jcp.29321
35. Sun S, Zhang M, Lin J, Hu J, Zhang R, Li C, Wei T, Sun D, Wei J, Wang H. Lin28a protects against diabetic cardiomyopathy via the PKA/ROCK2 pathway. Biochem Biophys Res Commun 2016;469:29-36. https://doi.org/10.1016/j.bbrc.2015.11.065
36. Zhang M, Niu X, Hu J, Yuan Y, Sun S, Wang J, Yu W, ET AL. Lin28a protects against hypoxia/reoxygenation induced cardiomyocytes apoptosis by alleviating mitochondrial dysfunction under high glucose/high fat conditions. PLoS One 2014;9:e110580. https://doi.org/10.1371/journal.pone.0110580
37. Sung Y, Jeong J, Kang RJ, Choi M, Park S, Kwon W, Lee J, ET AL. Lin28a expression protects against streptozotocin-induced beta-cell destruction and prevents diabetes in mice. Cell Biochem Funct 2019;37:139-147. https://doi.org/10.1002/cbf.3376
38. Song P, Chen Y, Liu Z, Liu H, Xiao L, Sun L, Wei J, He L. LncRNA MALAT1 Aggravates Renal Tubular Injury via Activating LIN28A and the Nox4/AMPK/mTOR Signaling Axis in Diabetic Nephropathy. Front Endocrinol 2022;13:895360. https://doi.org/10.3389/fendo.2022.895360
39. Guiot J, Henket M, Remacle C, Cambier M, Struman I, Winandy M, Moermans C, ET AL. Systematic review of overlapping microRNA patterns in COVID-19 and idiopathic pulmonary fibrosis. Respir Res 2023;24:112. https://doi.org/10.1186/s12931-023-02413-6
40. Cai P, Mu Y, Olveda RM, Ross AG, Olveda DU, McManus DP. Serum Exosomal miRNAs for Grading Hepatic Fibrosis Due to Schistosomiasis. Int J Mol Sci 2020;21:3560. https://doi.org/10.3390/ijms21103560
41. Shi M, Cui H, Shi J, Mei Y. mmu-microRNA-92a-3p attenuates pulmonary fibrosis by modulating Cpeb4-mediated Smad2/3 signaling pathway. Funct Integr Genomics 2022;22:1297-1306. https://doi.org/10.1007/s10142-022-00879-z
42. Schroder K, Tschopp J. The inflammasomes. Cell 2010;140:821-832. https://doi.org/10.1016/j.cell.2010.01.040
43. Nathan C, Ding A. Nonresolving inflammation. Cell 2010;140:871-882. https://doi.org/10.1016/j.cell.2010.02.029
44. Fong CH, Bebien M, Didierlaurent A, Nebauer R, Hussell T, Broide D, Karin M, Lawrence T. An antiinflammatory role for IKKbeta through the inhibition of "classical" macrophage activation. J Exp Med 2008;205:1269-1276. https://doi.org/10.1084/jem.20080124
45. Liu YC, Zou XB, Chai YF, Yao YM. Macrophage polarization in inflammatory diseases. Int J Biol Sci 2014;10:520-529. https://doi.org/10.7150/ijbs.8879

46. Murphy CA, Langrish CL, Chen Y, Blumenschein W, McClanahan T, Kastelein RA, Sedgwick JD, Cua DJ. Divergent pro- and antiinflammatory roles for IL-23 and IL-12 in joint autoimmune inflammation. J Exp Med 2003;198:1951-1957. https://doi.org/10.1084/jem.20030896